J. Astrophys. Astr. (1990) **11**, 237–253

An Observational Constraint on the Existence of Proto-Superclusters at z =3.3

Ravi Subrahmanyan & G. Swarup *Radio Astronomy Centre, Tata Institute of Fundamental Research, Post Box 8, Ootacamund 643001, India*

Abstract. Observations have been conducted using the Ooty Radio Telescope in order to place constraints on the evolutionary scenario leading to the formation of the present day superclusters. The experiment attempted to detect 21 cm emission from massive neutral hydrogen condensates at a redshift of z = 3.3. In an Einstein de-Sitter universe with baryon density Ω = 0.05, about ten condensates were expected in the volume surveyed if superclusters, having H I masses $\simeq 5 \times 10^{15}\ M_{\odot}$, were the first objects to separate out of the Hubble expansion. The sensitivity of our experiment rules out the existence of these condensates at z = 3.3 unless their lifetimes are less than one-tenth the dispersion in their epoch of formation or the proto-superclusters subtend angles greater than 6 arcmin. The result indicates that superclusters form at $z > 3.3$ if indeed they were the first objects to condense out of the Hubble flow.

Key words: Clusters of galaxies, formation—HI observations—HI regions, cosmological—protoclusters—superclusters, formation

1. Introduction

If hot dark matter dominates the mean matter density in the Universe, adiabatic density perturbations are expected to have resulted in the formation of massive gaseous condensates which subsequently fragmented and formed the clusters and galaxies. At redshifts when these predicted progenitors of the present-day galaxy clusters and superclusters are expected to be predominantly neutral gas condensates of primordial composition, they should be 'visible' to us in their 21 cm emission. Following the theoretical predictions of Sunyaev & Zel'dovich (1972), Novokreshchenova & Rudnitskii (1973) and Sunyaev & Zel'dovich (1974), the first observing programme attempting to detect redshifted 21 cm emission from protoclusters at z = 3.33 and 4.92 was conducted by Davies, Pedlar & Mirabel (1978) using the Jodrell Bank Mk 1A telescope. Hogan & Rees (1979) computed the observable properties of H I gas having an inhomogeneous distribution with a clustering scale at high redshifts estimated using the present day galaxy two-point correlation length and an adopted growth rate for the fluctuations. Bebbington (1986) used the Cambridge 6C telescope and searched the entire sky north of 82° declination in an attempt to detect primordial pancakes at a redshift of z = 8.4. Motivated by the possibility of discovering primordial H I condensates, de Bruyn *et al.* (1988) as also Hardy & Noreau (1987) conducted sensitive observations with the Westerbork and Very Large Array Telescopes respectively adopting spectral-line Fourier-synthesis techniques in fields

devoid of strong continuum radio sources. More recently, the spectral appearance of this emission from H I at high redshifts has been theoretically discussed by Subrahmanyan (1990) for a variety of plausible matter distributions.

All observational efforts towards the detection of redshifted 21 cm emission/absorption from inhomogeneities in the primordial neutral gas at epochs prior to the 'first light'—emission of optical radiation from the first 'stars'—have so far been unsuccessful. They have been useful in deriving constraints on the nature of the Universe at high redshifts and consequently on the possible scenarios that lead to the formation of the galaxies and the observed large scale structure of the present-day Universe. The importance of knowledge regarding the state of the Universe during the 'dark ages' led us to attempt an experiment that has resulted in improved constraints on the scenario leading to the formation of clusters and superclusters. Our interpretations of the observational results have stronger implications as compared to those of previous workers. We have conducted complementary observations using the Ooty radio telescope and the Very Large Array (VLA). The Ooty experiment encompassed a greater search area with a larger velocity depth and was designed to seek evidence for the most massive structures theoretically expected, in which the velocity dispersions are the highest. The VLA experiment had higher spatial and velocity resolutions and attempted to detect smaller-mass isolated structures and also signatures of a patchy H I distribution. The observational results obtained with the Ooty Radio Telescope form the subject matter of this paper. The observations with the VLA are discussed in an accompanying paper (Subrahmanyan & Anantharamaiah 1990).

Our searches were conducted at a frequency of 326.5 MHz corresponding to the receipt of 21 cm emission from a redshift of $z = 3.35$. This choice of search redshift was primarily constrained by the operating frequency of the ORT. Discoveries of examples of ongoing galaxy formation at low redshifts (Bothun *et al.* 1987; Bergvall & Jorsater 1988) and primeval galaxy candidates at redshifts $z \sim 2$–3 (Djorgovski *et al.* 1987; McCarthy *et al.* 1987; Chambers, Miley & van Breugel 1988) suggest that galaxy formation is an extended process which may begin at high redshifts but continues to the present day. The existence of forming galaxies at low redshifts suggests that our search-redshift of $z = 3.3$ could contain H I condensates where star formation is yet to commence. We adopt the Hubble constant $H_0 = 75$ km s^{-1} Mpc^{-1} and the density parameter $\Omega_0 = 1$ throughout this paper while relating the observables to physical quantities in the emitter frame. A line-of-sight velocity dispersion of Δv (km s^{-1}) in an H I region at a redshift of $z = 3.35$ causes the observed line profile to have a width

$$\Delta\nu_0^{\nu} = 1.09\ (\Delta v/1000\ \mathrm{km\,s^{-1}})\ \mathrm{MHz}. \tag{1}$$

Line emission from an optically-thin cloud at $z = 3.35$ having an H I mass $M_{\mathrm{H\,I}}$ will be observed with a peak flux density (Subrahmanyan 1990)

$$S_{\mathrm{p}} = 6.4\ (M_{\mathrm{H\,I}}/10^{14}\,M_{\odot})(\Delta v_0/1\ \mathrm{MHz})^{-1}\ \mathrm{mJy}. \tag{2}$$

2. The observations with the Ooty Radio Telescope

All the observations discussed here were conducted over the period June 6 to August 16, 1988 using the Ooty Radio Telescope (ORT; Swarup *et al.* 1971; Joshi *et al.* 1988). The observations were made during the period between 1800 and 0800 hrs local time,

with the bulk of data acquired during the night in order to avoid spurious spectral responses as a result of the Sun appearing through distant sidelobes of the telescope beam. In addition, interference due to activities in the neighbourhood of the telescope site was less at night. The ORT antenna consists of a parabolic cylindrical reflector with its axis in the north-south direction and with a dipole array feed along the focal line. The beam is steered in hour-angle by mechanical rotation with pointing in declination being achieved by electrical phasing of the array. Multiple beams are simultaneously formed on the sky by separately combining the signals from the feed elements with suitable delays and phase shifts. The telescope, along with the associated receiver system, was configured to simultaneously provide a 64-point spectrum over a 9.216 MHz bandwidth centred at 326.5 MHz towards each of four regions of the sky, which are defined by four beams of the telescope.

The spectra were obtained as the discrete Fourier transforms of the cross-correlation between the signals from the northern and southern halves of the north-south ORT aperture; the cross-correlation measurements being computed at discrete delay values. Hence the spectra are complex with the real and imaginary components having point source responses of the form

$$V_R(\sigma) \sim \frac{\sin^2(\pi\sigma \cdot \mathbf{U}_\lambda)}{(\pi\sigma \cdot \mathbf{U}_\lambda)^2} \cos(2\pi\sigma \cdot \mathbf{U}_\lambda)$$

and

$$V_I(\sigma) \sim \frac{\sin^2(\pi\sigma \cdot \mathbf{U}_\lambda)}{(\pi\sigma \cdot \mathbf{U}_\lambda)^2} \sin(2\pi\sigma \cdot \mathbf{U}_\lambda) \tag{3}$$

respectively in the north-south direction. In these expressions U_λ is the baseline vector (with a length, in units of wavelengths at the observing frequency, corresponding to the distance between the phase centres of the two halves of the north-south continuous aperture of ORT) and σ (radians) is a celestial position vector with origin on the celestial sphere at the celestial position towards which the beam is pointed. The quantity $1/U_\lambda$ corresponds to 12.5 sec δ arcmin. The real and imaginary component spectra pertain to orthogonal beam patterns that together cover a primary beam having half power beam widths (HPBW) of 2°.2 in east-west and 11.1 sec δ arcmin in north-south directions. The adjacent beams are separated in declination by 9 secδ arcmin. Response to sources having angular scales exceeding ≈ 6 arcmin would be severely attenuated in the correlation beams.

The H I condensates are expected to manifest themselves as position dependent spectral features. When one of the antenna beams is pointed towards an arbitrary celestial position, the telescope provides a complex spectrum that contains flux contributions from the sources lying in the field, sources lying outside the field that are seen through the beam sidelobes and grating lobes, and spurious responses arising from the coupling of signals into the two halves of the telescope that constitute the interferometer pair. Each of these contributions are modified by the bandpass characteristics of the receiver electronics that they traverse. In order to cancel all the spurious additive signals that are generated within the telescope receiver system, we have chosen to take a difference of the spectra obtained for each beam from a pair of fields on the sky. This beam-switching was performed by slewing the telescope antenna in hour angle between two fields keeping the declination setting (phasing of

the array) unchanged because changing the telescope declination setting entails a change in the signal pathway and consequently the spurious responses will be altered. Correction for the bandpass characteristics was performed by calibrating the observed spectrum using the spectral response obtained on a strong continuum source, the bandpass calibrator. The pair of fields have been selected so that their declinations are identical to the declination of the calibrator at the observing epoch. Since four beams of ORT which are separated in declination are simultaneously used, only one of these beams will have a declination identical to that of the calibrator. Hence only one of the beams will be perfectly calibrated without any change of declination setting. Calibration of the remaining three beams requires a small (< 18 sec δ arcmin) declination change and consequently these beams will suffer a small calibration error. The spurious spectral features arising as a result of this calibration error are negligible in comparison with the spurious spectral features arising due to distant background continuum sources appearing through the ORT antenna grating lobes.

Every field-pair was observed for 4 to 6 sessions (nights) of ~ 6 hours each so as to accumulate a minimum of ~ 20 hours of interference-free data on each field-pair. The bandpass calibrator was observed once for every session; data being acquired with each of the four beams being pointed sequentially on the source for 5–10 min. The calibrator flux density and observing duration were chosen sufficiently large so as to obtain a higher signal-to-noise ratio on the calibrator as compared to that on the difference spectra obtained for each session. The field-pair was observed, with data being acquired for 10 min on each of the fields alternately, by slewing the antenna in hour angle. The data acquired in an observing session was calibrated using the observations of the calibrator made during the same session. The normalized complex bandpass frequency response in each of the four beams displayed < 5 per cent peak variations over the few days period encompassing the 4–6 sessions that were devoted to observations on a single field-pair. On a few occasions when the calibrator data for a particular session could not be obtained—owing to the telescope becoming inoperative prior to the completion of the calibration scan—the data were calibrated using the bandpass response obtained on an adjacent night's observation, with an overall multiplicative correction factor applied based on the relative telescope sensitivity.

Careful off-line data rejection was required in order to eliminate interference. Since the fields are chosen to be devoid of sources $\geqslant$1 Jy, no signal is expected at the 2σ level in the 20-s integrated spectra that are obtained during observations on the field-pair. Hence, these data records were scanned and those containing spectra with peaks exceeding the expected rms thermal noise by a factor ~ 4 were rejected. Since the beams are formed by offset-phasing of the array, interference does not appear with equal prominence in all the beams. Therefore, whenever peaks exceeding the 4σ limit were detected in any one beam, the data on all the four beams were rejected during that integration period. On the average, data for ~ 15 per cent of the observing duration was lost due to interference. Prior to the averaging of all the thirty 20-s integrated complex spectra within a 10-min scan duration, an rms-amplitude (σ_a) was computed for all the 64 × 30 = 1920 spectral measurements and values exceeding a $2.5\sigma_a$. limit were excluded from the averaging. Typically $\geqslant$1 per cent of the points were eliminated by this procedure.

The correlation coefficient measured between the signals from the two halves of the telescope antenna, when observing the unresolved continuum calibrator, varied between 0.17 per cent to 0.21 per cent per Jansky flux density. Adopting a value of

240 K for the system temperature, the implied sensitivity for each half of ORT is between 0.4 and 0.5 K Jy^{-1}.

A total of 12 pairs of regions were surveyed in the beam-switching mode. Since four beams of the ORT were used, the total search area corresponding to 96 beam areas is 33.2 square degrees. The useful bandwidth is 8.5 MHz centred at the operating frequency of 326.5 MHz. For each field-pair, each beam yields a complex difference-spectrum whose real and imaginary components pertain to orthogonal beam patterns. Hence, we have obtained a total of 96 independent real difference-spectra.

Within the right ascension and declination range visible to the telescope at night during the observing months, and lying off the galactic plane, a list of candidate calibrator sources was prepared by including all the sources that have a flux density $\geqslant$ 10 Jy at 327 MHz and, in addition, were unresolved by the ORT correlation beam. The fields were now constrained to lie on declination strips having precessed declination coordinates identical to that of the candidate calibrators. The major cause for spurious spectral features in ORT are continuum sources lying at the positions of the antenna grating lobes. These spectral features arise because the grating lobe positions are themselves frequency dependent. The quality of a field was hence determined by the relative paucity of sources at the grating-lobe positions. Fields having strong sources in the main lobe were also avoided. The radio source catalogue which was scanned for confusing sources was constructed by merging non-overlapping sections of the 408 MHz Molonglo survey (Large *et al.* 1981), the 365 MHz Texas catalogue (Douglas *et al.* 1979) and the 408 MHz galactic plane survey by Clark & Crawford (1974). The telescope beam was arrived at by actual observations of a strong source through the grating lobes. With the pair of fields constrained to have a separation in hour-angle between 3°.75 and 7°.5 in order to minimize the time that is lost during the slew between successive scans, a final list of 12 pairs of fields was arrived at by an assessment of the relative confusion levels at positions along the allowed declination strips.

In order to obtain a rough estimate of the nature of spectra expected to be observed as a consequence of sources lying in the grating lobes, we computed theoretical spectra for the two positions corresponding to the field-pair number 12. These spectra are essentially a sum of the contributions made at each frequency channel by sources, in the catalogue described above, that lie in the main or grating lobe positions. Peak-to-peak variations of about 100–150 mJy are seen, and the channel-to-channel fluctuations in the flux density have an rms value of ~ 30 mJy. This figure represents a pessimistic estimate of the telescope confusion limit for broadband spectral-line work. Due to our lack of precise knowledge regarding the amplitude and phase responses in the individual grating lobes, we cannot overcome this limitation arising from continuum sources by attempting to eliminate their effects by a subtraction of the theoretical spectra from the observed spectra.

In Table 1 we have listed the 1950.0 epoch coordinates of the twelve field-pairs observed. Both right ascension and declination as well as Galactic coordinates are listed along with the total useful interference-free observing duration on each field-pair. These coordinates pertain to the positions of the third beam used. The first two and the fourth beams occupy adjacent positions to the south and north respectively. The amount of data rejected was roughly equal for both the fields in any field-pair and hence half the listed time constitutes the useful observing duration on each field. For each of the twelve pairs of regions, a calibrated complex difference spectrum was

Table 1. The field pairs observed with the ORT.

Field pair	RA (1950)	DEC (1950)	l	b	T (hrs)
1	14 26 55.0	−10 55 44	−21.93	44.92	20.9
	14 44 54.2	−10 56 22	−16.85	42.47	
2	14 27 04.8	07 14 10	−3.40	59.24	19.9
	14 45 05.1	07 13 32	2.14	55.90	
3	14 40 13.8	21 37 31	26.26	64.11	17.9
	15 00 15.0	21 36 46	29.30	59.68	
4	15 32 05.3	06 39 30	12.45	46.15	22.4
	15 52 05.5	06 38 34	16.11	41.94	
5	21 38 57.4	−05 11 15	50.34	−39.70	19.2
	21 58 57.8	−05 11 52	53.93	−43.91	
6	20 41 11.3	15 56 44	61.04	−15.96	21.9
	20 58 10.6	15 56 01	63.57	−19.25	
7	20 49 56.5	−05 09 25	42.95	−29.12	24.5
	21 06 56.8	−05 10 06	45.34	−32.83	
8	20 39 02.7	03 53 07	50.10	−22.21	21.6
	20 58 02.5	03 52 19	52.88	−26.21	
9	22 37 53.2	−20 58 02	37.93	−59.51	20.8
	22 57 54.9	−20 58 24	41.17	−63.93	
10	20 39 06.9	09 51 14	55.48	−19.00	22.4
	20 58 06.4	09 50 27	58.31	−22.86	
11	20 39 48.9	−15 32 16	30.87	−31.40	20.0
	21 06 50.1	−15 33 23	33.92	−37.40	
12	22 41 55.4	−15 36 13	48.23	−58.30	25.1
	23 00 56.6	−15 36 32	52.62	−62.33	

computed corresponding to each of the four beams used. The real and imaginary components of these spectra obtained on the four beams for the twelfth pair of fields is displayed as an example in Fig. 1.

3. Data analysis and results

The search with the Ooty radio telescope has been-an attempt to detect signatures of massive H I condensates in the search volume located at the redshift of z = 3.35. The condensates are expected to manifest themselves as redshifted emission lines which would appear as either emission or absorption features in the difference spectra depending on their location in the pair of fields observed in the beam-switching mode. If condensates are present in both the fields, with the same Hubble velocity as well as position with respect to the field centres, their responses will cancel in the difference spectrum. However, the probability of such an occurrence is expected to be small. The procedure described below was adopted for detecting features in the spectra as it gives the most likely value for the amplitude of a feature of a specified width that is present at each location in the difference spectra.

We first decompose the 'difference spectrum' into a 'smooth spectrum' and a 'residue component'. We have represented the smooth spectrum by a cubic-spline function (Schwab 1983). Our procedure consists of firstly computing a spline fit using the method of cross validation. In the presence of spiky spurious signals in the

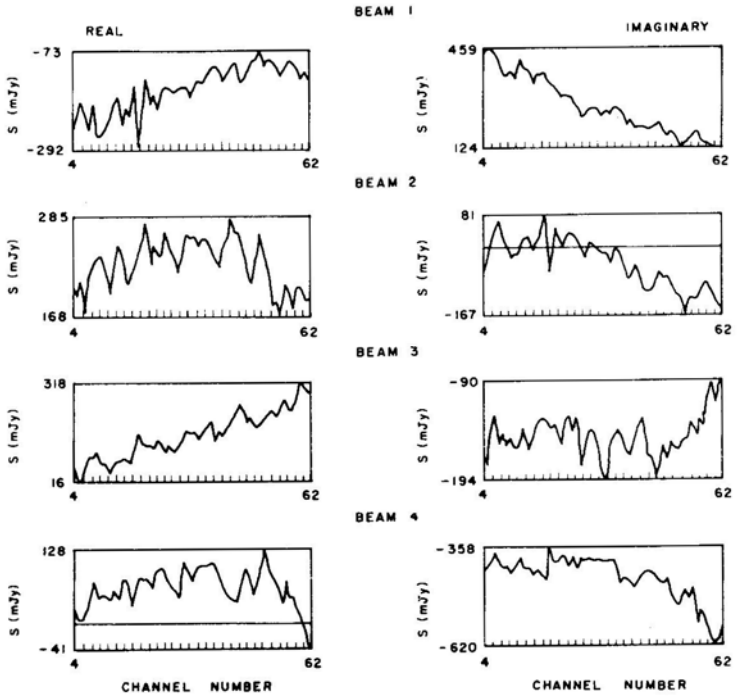

Figure 1. The real and imaginary components of the complex difference spectra obtained on differencing the observations on each of the four beams for the field-pair 12. The spectra are plotted in units of mJy flux density as a function of channel number.

spectrum, which could have arisen from interference, this fit would recognize the narrow features as untrue and the resulting smooth spectrum would not be influenced by interference present in the difference spectrum. If the cross-validation method for the determination of the smoothing parameter fails, as evidenced in the rms noise of the residue component having a value lower than the expected thermal noise, we repeat the spline smoothing with the smoothing parameter fixed so that the rms value of the residue component is equal to the specified thermal noise. The decomposition is illustrated in Fig. 2. The continuous curve is the difference spectrum and the smooth spectrum is shown as a dashed line.

We next performed a search for features having Gaussian profiles with widths corresponding to velocity dispersions of 600, 900, 1200, 1800 and 2400 km s^{-1}. At every point in the spline-smoothed spectrum for each such search, we demarcate, as a 'signal domain', a neighbourhood centred at the point of current interest and having an extent that is twice the full width at half maximum (FWHM) of the features that we seek to detect. Considering the point corresponding to channel number 36 in Fig. 2, the signal domain is the region marked S. The 'interpolated baseline' in this signal domain is determined by performing a second-order polynomial-interpolation from a pair of segments of the smooth spectrum, which adjoin the signal domain on either side, and each of which have a length that is at most equal to the extent of the signal domain. In Fig. 2, interpolation from regions R_1 and R_2 that adjoin the region S have yielded the baseline shown as a dot-dashed curve within the signal domain. This

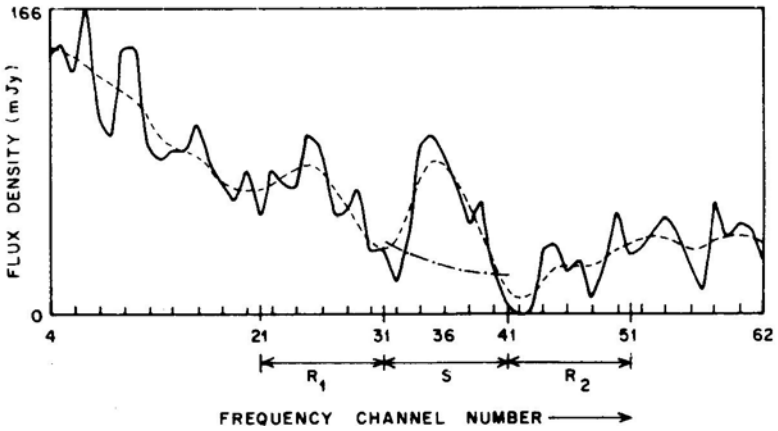

Figure 2. An illustration of the spectral segments involved in the search for signals. The continuous curve shows the difference spectrum and the dotted curve shows the smooth spectrum; both being plotted as a function of channel number. For the point of interest (channel 36), the range of channels marked S is the signal domain while the segments marked R_1 and R_2 are the remainder regions; the demarcation is valid for a search for a feature having a velocity dispersion of 600 km s^{-1}. The dot-dashed curve is the interpolated baseline.

baseline is subtracted from the difference spectrum in the signal domain to obtain a 'residue' version of this spectral segment. The best-fit amplitude of a template Gaussian, that has the required FWHM and whose truncated tail-end points are placed on the smooth-spectrum at the two boundaries of the signal domain, is computed by a weighted least squares fit to the residue difference-spectrum within the signal domain. Spikes in the difference spectrum, that deviate significantly from the smooth spectrum and occur in those frequency channels where interference was noticed during data rejection, are given a weight of zero. The Gaussian fit smoothes over sharp fluctuations in the difference spectrum, which arise from the thermal noise and from interference, that have characteristic widths which are much smaller than the Gaussian width. The subtraction of the interpolated baseline ensures that high-amplitude low-order baselines, which could arise due to continuum sources being present in low order sidelobes, make a very diminished contribution to the amplitude estimate.

For each complex difference spectrum, the procedure detailed above was repeated at all the frequency channel locations separately for the components of the complex spectrum. Those points located within a FWHM of the ends of these spectra were excluded. The maximum of the absolute values of the best-fit amplitudes obtained at each frequency channel location on the component spectra was deemed to be the amplitude estimate at that location in the complex difference spectrum. A few fields that showed obvious effects of confusion arising from antenna grating lobe responses were trimmed in spectral extent to reject the affected frequency channels. Hence, a set of amplitude estimates were separately obtained at all the frequency channel locations in each of the 48 complex difference spectra observed. Histograms of the amplitude estimates were computed by binning all the amplitudes into 10 mJy-wide flux density bins. The number of amplitudes obtained in each bin was normalized by the number of amplitude estimates computed within a FWHM of the template Gaussian. The

histograms are displayed in Fig. 3. A continuous curve having a Rayleigh distribution is superimposed on each histogram as a reference. The flux density corresponding to the peaks of the Rayleigh forms are approximately the 1σ (1 standard-deviation) values of the amplitudes. The 1σ values are larger at larger velocity dispersions because of the presence of low-order baselines in the difference spectra as seen in Fig. 1. Although the detected amplitudes have an rms value that are mostly a factor of $\sim$ 3–7 higher than the expected rms thermal noise, we do not consider the search as having successfully detected proto-superclusters. These large deviations from the expected thermal noise arise as a consequence of the telescope grating responses. Hence, the spectra are basically confusion limited, and the 1σ amplitudes only reflect the confusion limit of the observations. The histograms roughly follow the Rayleigh form with no significant high-amplitude tails. Hence, we only infer upper limits on the existence of proto-superclusters in the search volume. The results are summarized in Table 2. For each velocity dispersion, the total comoving survey volume and the mean mass enclosed in a resolution element (volume defined by the HPBWs of the telescope beam and the FWHM of the template Gaussian) assuming closure density are listed in the table. The flux densities corresponding to the peaks of the Rayleigh forms and the corresponding H I masses are also listed. The 1σ of the amplitudes roughly correspond to H I masses that are a factor of 10 smaller than the closure-density mass expected in the resolution volume elements. These H I masses represent 1σ limits on the existence of proto-superclusters within the search volume at the redshift z = 3.3

4. Interpretation of the observational results

The search covers an area of the celestial sphere corresponding to 1.734×10^5 Mpc^2 at z = 3.35 and the useful bandwidth corresponds to a depth of 49.45 Mpc in comoving coordinates. The total comoving search volume is 8.6×10^6 Mpc^3. A 2.6 per cent redshift range has been covered around the redshift z = 3.35. Spherical condensates whose parent perturbations turn around at $z_t \approx 7$ and virialize at $z_v \approx$ A.3 would possess virialized radii $r_v \geqslant 2\ (\mathrm{M}/10_{16}\ M_\odot)^{1/3}$ Mpc resulting in their observed line profiles having widths $\Delta v_0^v \geqslant 0.6\ (\mathrm{M}/10^{14}\ M_\odot)^{1/3}$ MHz (Subrahmanyan 1990). For masses in the range 10^{14}–$10^{16}\ M_\odot$, the observed line-width is expected to have values ranging from several hundred kHz to a few MHz. Although objects having the virialised radii estimated above would subtend angular sizes of $\Delta\theta \geqslant 16\ (M/10^{16}\ M_\odot)^{1/3}$ arcmin, subsequent to collapse and virialization only the central

Table 2. 1σ upper limits on the H I masses of condensates at z = 3.3.

Δv km s^{-1}	Comoving survey volume h_{75}^{-3} Mpc^3	Closure mass in a resolution element $h_{75}^{-1}\ M_\odot$	1σ amplitude mJy	1σ upper limits on $M_{\mathrm{H\,I}}$ $h_{75}^{-2}\ M_\odot$
600	7.2×10^6	2.1×10^{15}	20	2.0×10^{14}
900	7.0×10^6	3.1×10^{15}	22	3.4×10^{14}
1200	6.8×10^6	4.2×10^{15}	23	4.7×10^{14}
1800	6.0×10^6	6.2×10^{15}	30	9.2×10^{14}
2400	5.4×10^6	8.3×10^{15}	42	1.7×10^{15}

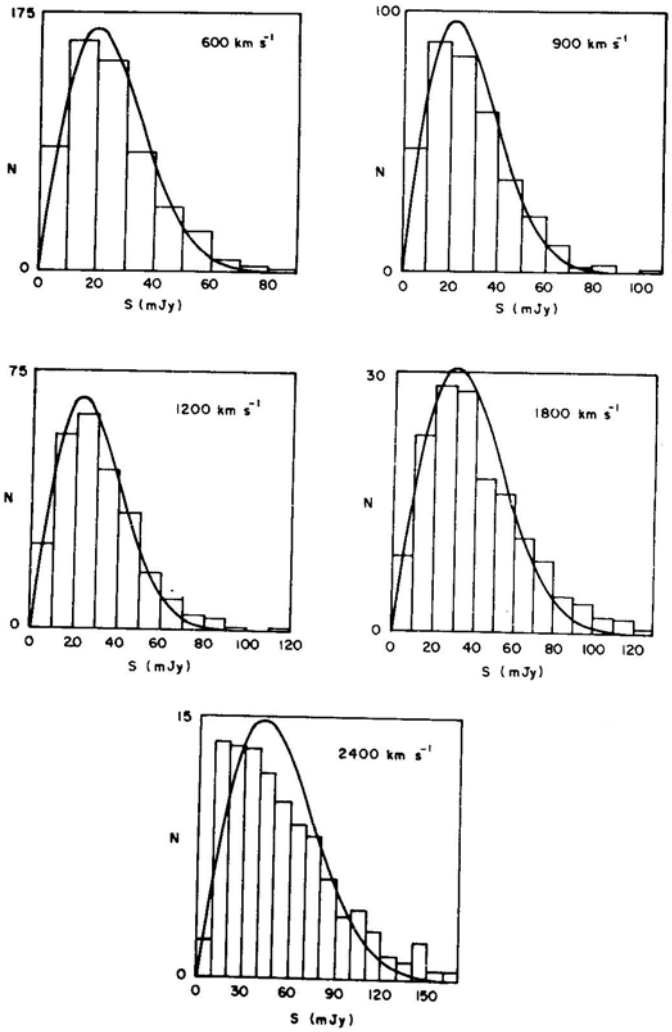

Figure 3. Histogram display of the amplitudes detected in the difference spectra. Each histogram pertains to features having a specific velocity dispersion as indicated in the plots. The continuous curves are Rayleigh distribution functions that have been plotted as a reference.

dense regions that cool rapidly are expected to abound in H I. Hence, the 21 cm line-emitting region would subtend an angle of a few arcmin. The ORT, when operated as a two-element interferometer as in this search experiment, is sensitive to structures $\leqslant$ 6 arcmin. If the condensates have the form of oblate pancakes, with the dense H I being in a sheet having a size as large as the longest dimension of the pancake, our search would fail to detect the pancakes if they were observed face-on. When observed edge-on, the velocity dispersion along the line-of-sight would approximately equal the differential Hubble velocity across the length of the pancake. This leads to an observed line width of $\Delta\nu_o^H \approx 1.5\ (M/10^{14}\ M_\odot)^{1/3}$ MHz and this could be as large as several MHz for supercluster mass pancakes. Hence, although proto-superclusters

having spherical or prolate structures can be detected in our search, highly flattened pancakes may well escape detection.

4.1 *Interpretation of the Cumulative Histograms*

In order to facilitate a comparison with the predictions from the theoretical scenarios of galaxy formation, the data have been presented in the form of cumulative histograms in Fig. 4. The bins along the *x*-axis are in units of solar masses of H I gas. Each plot corresponds to structures of a specific velocity dispersion, and the height of each histogram-bar is an upper limit to the mass fraction contained in proto-superclusters

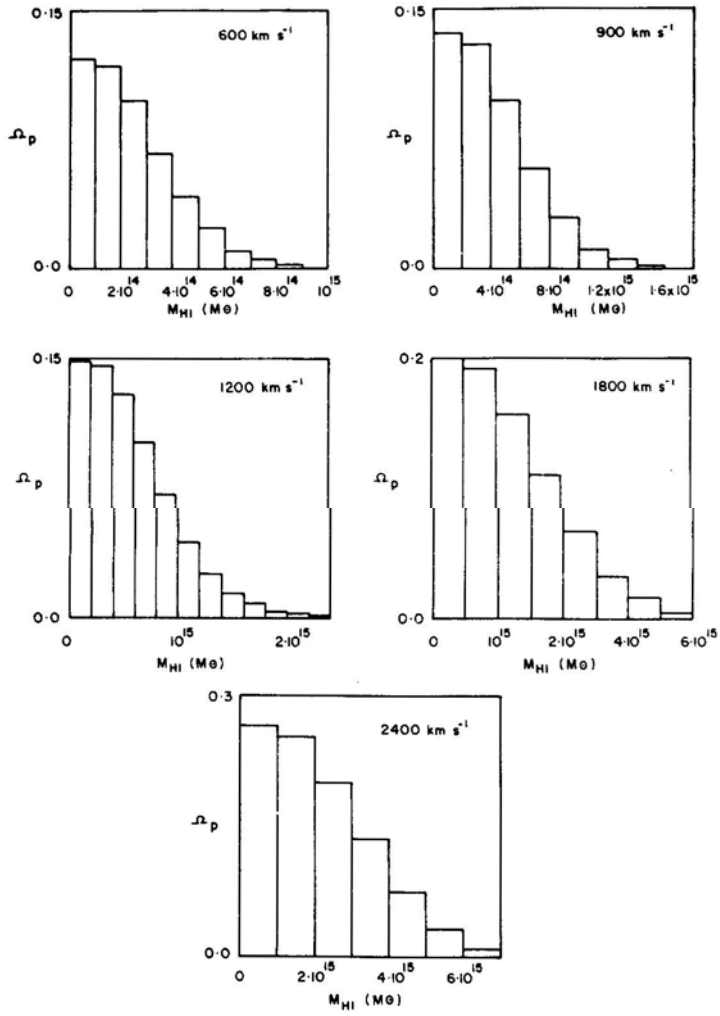

Figure 4. Cumulative histogram display of the amplitudes detected in the difference spectra. The heights of the histogram-bar denote upper limits on the fraction of the closure-density mass that can reside in H I condensates having masses exceeding the bar ordinate.

of mass exceeding the bar abscissa. This cumulative H I mass is expressed as a fraction, Ω_p, of the total closure-density mass expected within the search volume. From the maximum of the heights of histogram bars of Ω_p, we can rule out scenarios where $\geqslant 0.2$ of the closure density of the Universe exists as 'visible' proto-superclusters at the redshift $z = 3.3$. The observational limits on the Gunn-Peterson test have been used to infer upper limits on the baryon fraction Ω_B that are significantly smaller than our limit (Steidel & Sargent 1987). Nevertheless, our limit is based on a direct attempt to detect clumpy H I at $z = 3.3$ in its 21 cm emission and is important in the light of recent work suggesting that the observed abundances of light elements could imply primordial nucleosynthesis with $\Omega_B = 1.0$ (Maloney & Fowler 1988).

The maximum number of structures (N_m) of any arbitrary mass M that are expected to be present in the entire search volume is given by the ratio of the total closure-density mass expected to be present in the volume to the mass M. An upper limit to the number actually present (N_0) is obtained by computing the cumulative number of flux density peaks corresponding to H I masses exceeding the mass M. A peak corresponding to any arbitrary mass M^*, with $M^* > M$, is counted as M^*/M number of masses. We assume that the baryon density parameter $\Omega_B \approx 0.1$ and that proto-supercluster lifetimes exceed one-tenth the dispersion in their epoch of formation (which includes z = 3.3). Then we would expect the observed number, No, to be larger than a fraction, 1/100, of the number N_m. For each velocity dispersion, we can now set an upper limit to the individual proto-supercluster mass as that value of M above which the number N_m exceeds the number that is allowed by the data by at least a factor of 100. From Fig. 4, we hence obtain upper limits that range from $6 \times 10^{14}\ M_\odot$ at a dispersion velocity of 600 km s^{-1} to a value of $6 \times 10^{15}\ M_\odot$ at the dispersion velocity of 2400 km s^{-1} on the H I masses of proto-superclusters. These limits are very nearly three times the 1σ limits obtained in Table 2. If we make a further assumption that 50 per cent of the gas in a proto-supercluster is neutral and that the gas has a composition which is 70 per cent hydrogen and 30 per cent helium by mass, we obtain corresponding upper limits on the total baryonic masses of individual proto-superclusters that are $1.7 \times 10^{15}\ M_\odot$ and $1.7 \times 10^{16}\ M_\odot$ at the dispersion velocities of 600 and 2400 km s^{-1} respectively. The limits at intermediate velocity dispersions lie within the range defined by these two values. If we relax the above assumption and accept as a limit the value of mass M at which the expected number is a factor of 10 larger than the number allowed by the data (in contrast to the factor 100 adopted previously), we obtain limits ranging from 2.3×10^{14} to $3.6 \times 10^{15}\ M_\odot$ of H I over the range of velocity dispersions 600 to 2400 km s^{-1}. These limits correspond to standard deviations between 1.1σ and 2.1σ of the detected peaks. These limits are relevant if the Universe contains baryonic matter of ≈ 10 per cent density and the proto-supercluster lifetimes are comparable to the dispersion in the epoch of their formation (which again includes $z = 3.3$).

4.2 *Implications of the Search Sensitivity and Volume*

In Fig. 5, we have compared the search volumes of all the experiments conducted at the redshift of $z = 3.3$. The figure provides the fiducial number of proto-superclusters of any fixed mass that could be present in each of the comoving search volumes by assuming that all the closure-density mass resident in the search volume is present as

proto-superclusters of the adopted mass. The horizontal lines denote the commoving search volumes of the Ooty, Westerbork (de Bruyn *et al.* 1988), VLA (Hardy & Noreau 1987), and Jodrell (Davies *et al.* 1978) observations. In Fig. 6, we have compared the 2a upper limits set by these different observations. Consistent with the constraints of primordial nucleosynthesis (Yang *et al.* 1984), we now assume that 5 per cent of the closure-density matter in the Universe is baryonic. We note from Fig. 5 that the Ooty observations cover a search volume that could have greater than 10 condensates if the individual condensate H I masses are less than $\approx 5 \times 10^{15}\ M_{\odot}$. Of these 10 condensates, only a fraction would be actually observable to us in their 21 cm emission depending on the dispersion in the epoch of formation of the condensates and their lifetimes in the neutral gaseous phase. For example, if the lifetimes are one-tenth of the dispersion in the formation epoch, and our search redshift is situated within the epochs of formation, we would expect to observe one-tenth of the total number of condensates resident in the search volume. Hence, in the case of condensates with $\approx 5 \times 10_{15}\ M_{\odot}$ in H I gas, we would expect to observe one proto-supercluster within the search volume. Comparing this expectation with the 2σ limits plotted in Fig. 6 and the histograms of the amplitudes in Fig. 3, we infer that not a single amplitude peak corresponding to a proto-supercluster having an H I mass exceeding $\approx 5 \times 10^{15}\ M_{\odot}$ has been detected within the search volume for dispersion velocities < 2000 km s^{-1}. Hence, under the assumptions stated above, the Ooty observations have the necessary sensitivity and search volume in order to place meaningful constraints on condensates at the redshift of $z = 3.3$ that have total masses $\approx 10^{17}\ M_{\odot}$. Larger mass condensates could be ruled out only if the assumed lifetimes exceed one-tenth the dispersion in the epoch of formation. Considering condensates of lower masses, we infer from Fig. 5 that the maximum number of condensates that could be expected within the search volume exceeds 10^2 for total masses $< 10^{16}\ M_{\odot}$. Adopting the same assumptions as discussed above, $\approx$ 10 proto-superclusters each having $\approx 5 \times 10^{14}\ M_{\odot}$ in H I gas are expected to be detected within the search volume. The sensitivity of the search indicates that condensates with H I masses $> 5 \times 10^{14}\ M_{\odot}$ do not exist at $z = 3.3$ with their expected space densities, but the sensitivity does not constrain the existence of condensates having H I masses $\leqslant 5 \times 10_{14}\ M_{\odot}$ for the assumptions adopted. Useful constraints can be inferred for lower mass condensates only if Ω_B exceeds 0.05. The search volume determines the value of the largest condensate mass on which meaningful constraints can be derived, while the search sensitivity determines the lowest condensate masses.

4.3 *Abell Clusters*

Abell clusters of richness class $R \geqslant 1$ have a local space density of $2.5 \times 10^{-6}\ h_{75}^{3}$ Mpc^{-3} (Bahcall & Soniera 1983). Assuming that this also represents the comoving space density of the counterparts of these rich clusters at the redshift $z = 3.3$, we expect a total of ~ 20 such objects within the comoving search volume of $8.6 \times 10^{6}\ h_{75}^{-3}$ Mpc^{3} encompassed by the Ooty observations. We now examine the 20 highest amplitude estimates obtained in the histograms in Fig. 3. At the velocity dispersion of ~ 900 km s^{-1}, similar to the observed velocity dispersions in the galaxy clusters today, all these 20 peaks have flux densities that correspond to H I masses exceeding $10^{15}\ M_{\odot}$ by at most a factor of 2, with all the other peaks being below this

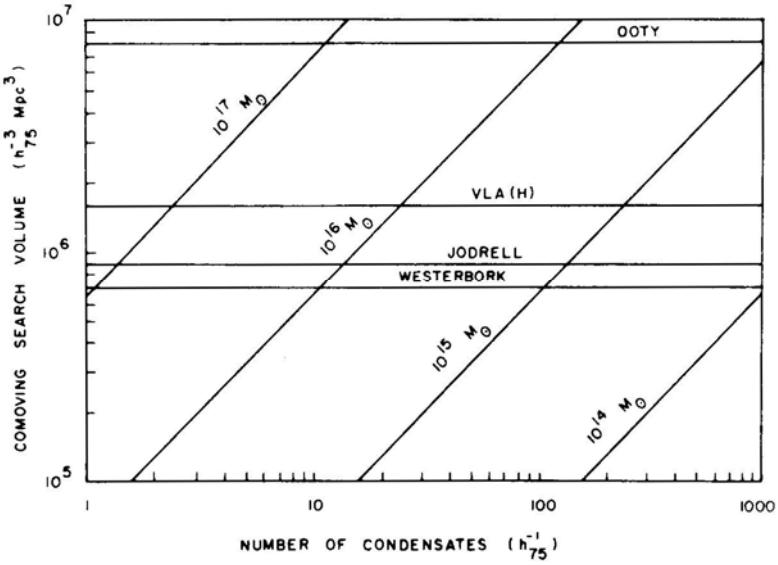

Figure 5. The relationship between the search volume and the expected number of proto-superclusters for various possible proto-supercluster masses. The assumption has been made that all the closure-density mass within the search volume is resident in proto-superclusters of a single mass. The horizontal lines represent the search volumes covered in various experiments.

mass limit. The rich clusters have total masses $\sim 7 \times 10^{14 \pm 1}\ h_{75}^{-1}\ M_\odot$ (Bahcall 1977). We infer that the richest Abell clusters, having $\geqslant 2 \times 10_{15}\ M_\odot$ in H I, do not seem to be present as neutral gaseous condensates at the redshift of $z = 3.3$.

4.4 *General Considerations*

The peak fluctuation expected, due to the system noise alone, depends on the number of independent measurements in the volume searched. Since the peak fluctuation expected is larger in searches covering larger volumes, the limits placed by an experiment that searches greater volumes will be poorer if the peak deviation is used to derive the upper limits. Hence, we have adopted the approach outlined in the preceeding paragraphs, where the limits would be better if larger volumes are surveyed. In our method of deriving limits, the expected number of structures exceeding an arbitrary mass M would be directly proportional to the volume surveyed. But the number allowed by the data, assuming that the data contains only Gaussian noise, would increase slowly with increasing number of measurements. This is because in a sample of N independent measurements of a Gaussian random variable (with standard deviation σ) the deviation x_m above which only one measurement is expected is given by the relationship: $\mathrm{erf}\,(x_m/\sqrt{2\sigma}) = (N - 1)/N$.

5. A comparison with earlier searches

The theoretical predictions of Sunyaev & Zeldovich (1974) suggest that our search volume should contain ~ 4 proto-superclusters and that the upper limit set by our

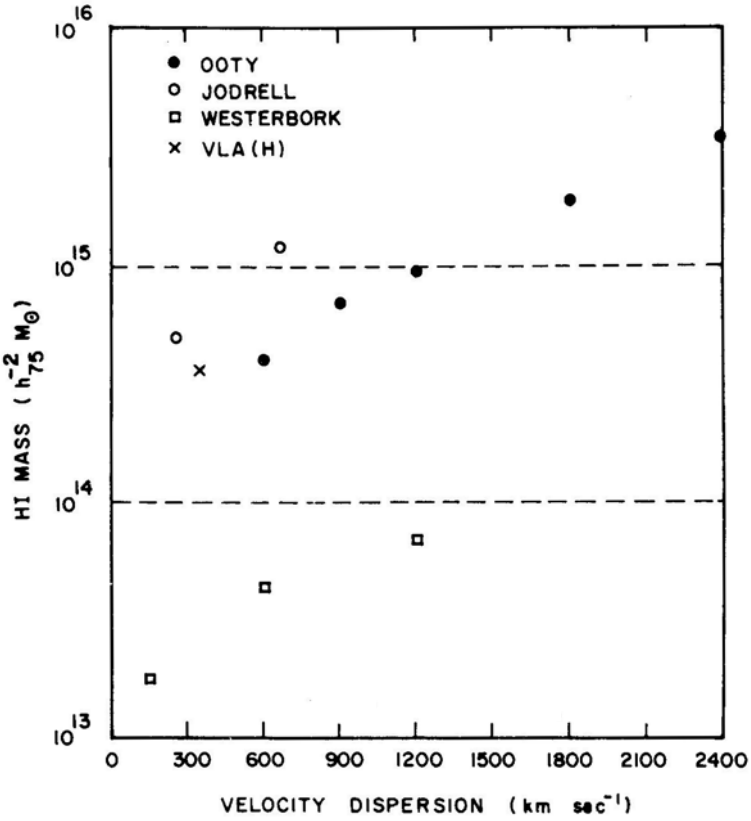

Figure 6. The 2σ limits on H I masses of protoclusters at the redshift of $z = 3.3$. The limits placed by various experiments are plotted as a function of the line-of-sight velocity dispersion. The implications of these limits for the formation of various large scale structures strongly depend on the comoving volume searched.

observations on the total mass of each proto-supercluster, derived using the same assumptions as used by Davies et al. (1978), is $2 \times 10^{15}\ M_\odot$. The observational upper limits presented in Fig. 2 of Davies et al. (1987) imply an upper limit of ≈180 mJy on the peak flux density from proto-superclusters having a velocity dispersion of 660 km s^{-1}. We infer the corresponding upper limit on the total mass of a proto-supercluster to be $6 \times 10^{15}\ M_\odot$ at $z = 3.3$. These observations conducted by Davies et *al.*, at the frequency corresponding to a search at the redshift of $z = 3.3$, cover a total comoving search volume, as defined by the half-power areas of their telescope beam, in which only 0.4 proto-superclusters are expected. Hence their upper limit does not seem significant and is, in addition, a factor of three above our limit. The search for protoclusters that was conducted by Hardy & Noreau (1987) encompassed a volume that is a factor of 5 smaller than the Ooty observations and, in addition, had a relatively poorer sensitivity because their data were strongly affected by interference. Observations conducted using the Westerbork Telescope (de Bruyn et al. 1988) attained rms noise levels that were an order of magnitude better than the Ooty observations. But the comoving search volume, encompassing ≈ 6–7 × $10^5\ h_{57}^{-3}$ Mpc^3, is an order of magnitude smaller than that covered by us at Ooty. In addition, the

restricted bandwidth used in the observations prevented searches for proto-superclusters that have line-of-sight velocity dispersions exceeding ≈ 1000 km s^{-1}. Their observations constrain the evolution of smaller mass entities whose dispersion velocities are less than ≈ 1000 km s^{-1} We interpret the 2σ flux density limits set by Bebbington (1986) as implying 2σ upper limits of $2 \times 10^{15}\ h_7^{-\frac{2}{5}}\ M_\odot$ on the H I inhomogeneities at the redshift of $z = 8.4$ that have line-of-sight velocity dispersions ≈ 1600 km s^{-1}. These observations encompassed a search volume of $1.8 \times 10^7\ h^{-\frac{3}{5}}_{\frac{7}{7}}\mathrm{Mpc}^3$, which is by far the largest volume searched in any such experiment. The sensitivity of the search allows strong constraints to be placed on only the most massive supercluster scale condensates and the observations indicate that supercluster mass condensates (of ≈ $10^{17}\ M_\odot$ total mass) do not exist at the redshift of z= 8.4 as well.

6. Conclusions

1. Less than a fraction 0.2 of the closure density of the Universe exists as condensates which are 'visible' in 21 cm emission at the redshift $z = 3.3$.

2. The observations place 2σ limits in the range $4 \times 10^{14} - 3.5 \times 10^{15}\ h_7^{-2}\ M_\odot$ on the H I content of individual primeval condensates that have line-of-sight velocity dispersions in the range 600-2400 km This limit pertains to a comoving search volume of $8 \times 10^6\ h_7^{-3}$ Mpc^3 situated at the redshift of $z = 3.3$. In an $\Omega_B = 0.05$ Einstein-de Sitter universe, the observations indicate that proto-superclusters having total masses in the range 10^{16}–$10^{17}\ M_\odot$, with their baryonic content in the neutral gaseous phase, may not exist at the redshift $z = 3.3$.

The Ooty observations have the sensitivity and the survey volume required in order to place constraints on the evolution of superclusters. The results indicate that superclusters, if indeed they are the first objects that condense out of the Hubble flow (as would be expected in a hot dark matter dominated universe), probably form at redshifts $z > 3.3$.

Acknowledgements

We thank the staff of the Radio Astronomy Centre, Ooty, for their cooperation during the conduct of these observations and Dr K. R. Anantharamaiah for a critical reading of the manuscript.

References

Bahcall, N. A. 1977, *Ann. Rev. Astr. Astrophys.,* **15**, 505.
Bahcall, N. A., Soneira, R. M. 1983, *Astrophys. J.,* **270**, 20.
Bebbington, D. H. 0. 1986, *Mon. Not. R. astr. Soc.,* **218,** 577.
Bergvall, N., Jorsater, S. 1988, *Nature,* **331**, 589.
Bothun, G. D., Impey, C. D., Malin, D. F., Mould, J. R. 1987, *Astr. J.,* **94,** 23.
Chambers, K. C., Miley, G. K., van Breugel, W. J. M. 1988, *Astrophys. J.,* **327,** L47.
Clark, D. H., Crawford, D. F. 1974, *Aust. J. Phys.,* **27**, 713.
Davies, R. D., Pedlar, A., Mirabel, I. F. 1978, *Mon. Not. R. astr. Soc.,* **182,** 727.

de Bruyn, A. G., Wieringa, M. H., Katgert, P., Sancisi, R. 1988, in *IAU Symp. 132: Large Scale Structures of the Universe,* Eds J. Audouze, M. C. Pelletan & A. Szalay, D. Reidel, Dordrecht, p. 211.

Djorgovski, S., Strauss, M. A., Perley, R. A., Spinrad, H**.,** McCarthy, P. 1987, *Astr. J.,* **93,** 1318.

Douglas, J. N., Bash, F. N., Torrence, G. W., Wolfe, C. 1979, Univ. Texas Publ. Astr. No. 17.

Hardy, E., Noreau, L. 1987, *Astr. J.,* **94,** 1469.

Hogan, C. **J.,** Rees, M. J. 1979, *Mon. Not. R. astr. Soc.,* **188,** 791.

Joshi, M. N., Swarup, G., Bagri, D. S., Kher, R. K. 1988, *Bull. Astr. Soc. India,* **16,** 111.

Large, M. I., Mills, B. Y., Little, A. G., Crawford, D. F., Sutton, J. M**.** 1981, *Mon. Not. R. astr. Soc.,* **194,** 693.

Maloney, R. A., Fowler, W. A. 1988, *Astrophys. J.,* **333,** 14.

McCarthy, P. J., Spinrad, H**.,** Djorgovski, S., Strauss, M. A., van Breugel, W., Liebert, J. 1987, *Astrophys. J.,* **319,** L39.

Novokreshchenova, S. I**.,** Rudnitskii, G. M. 1973, *Astr. Zh.,* **50,** 877.

Schwab, F. R. 1983, VLA Scientific Memorandum No. 147.

Steidel, C. C., Sargent, W. L. W. 1987, *Astrophys. J.,* **318,** L11.

Subrahmanyan, R. 1990, *Mon. Not. R. astr. Soc.,* submitted.

Subrahmanyan, R., Anantharamaiah, K. R. 1990, *J. Astrophys. Astr.*, submitted.

Sunyaev, R. A., Zel'dovich, Ya. B. 1972, *Astr. Astrophys.,* **20,** 189.

Sunyaev, R. A., Zel'dovich, Ya. B. 1974, *Mon. Not. R. astr. Soc.,* **171,** 375.

Swarup, G., Sarma, N. V. G., Joshi, M. N., Kapahi, V. K., Bagri, D. S., Damle, S. H**.,** Ananthakrishnan, S., Balasubramanian, V., Bhave, S. S., Sinha, R. P**.** 1971, *Nature Phys. Sci.,* **230,** 185.

Yang, J**.,** Turner, M. S., Steigman, G., Schramm, D. N., Olive, K. A. 1984, *Astrophys. J.,* **281,** 493.